Discriminating stocks of striped red mullet (Mullus surmuletus) in the Northwest European seas using three automatic shape classification methods

Abdesslam Benzinou, Sébastien Carbini, Kamal Nasreddine, Romain Elleboode, Kélig Mahé

Discriminating stocks of striped red mullet (*Mullus surmuletus*) in the Northwest European seas using three automatic shape classification methods

Abdesslam Benzinou, Sébastien Carbini, Kamal Nasreddine

Ecole Nationale d'Ingénieurs de Brest ENIB, UMR CNRS 6285 LabSTICC
29238 Brest Cedex 03 (FRANCE)

Romain Elleboode, Kélig Mahé

Ifremer, Laboratoire Ressources Halieutiques
62321 Boulogne sur mer (FRANCE)

Abstract

Stock identification is of primarily importance for population structure assessment of economically important species. This study investigates stocks of striped red mullet using three automatic methods of stock identification based on otolith shape and growth marks. Otolith shape is known to be a promising approach for stock identification but interpreting patterns of variance is a difficult problem. In this study, images in reflected and transmitted light were acquired from 800 otoliths sampled in the Northwest European seas from South Bay of Biscay to North Sea. The growth marks are pointed out manually by an expert. The external shape of otoliths were automatically extracted by computer vision process and then three automatic classification methods were compared, two classical state-of-the-art methods based on Fourier descriptors and Principal Component Analysis (PCA), and a recently proposed method based on shape Geodesics. From

Email address: benzinou@enib.fr (Abdesslam Benzinou)

a methodological point of view, results show that the shape geodesic approach significantly outperforms other classical methods. From a biological point of view, this study shows that the population of striped red mullet in Northwest European seas can be divided in three geographical zones: the Bay of Biscay, a mixing zone composed of the Celtic Sea and the Western English Channel and a northern zone composed of the Eastern English Channel and the North Sea (67% of correct classification rate using both shape and growth pattern information). Moreover, it shows that for a given zone, two subsets of the same year have a lower variability in shape than two subsets from two consecutive years.
Keywords: Striped red mullet, otoliths, stock identification, year identification, shape analysis, Fourier descriptors, Principal Component Analysis (PCA), shape Geodesics

1. Introduction

Striped red mullet (*Mullus surmuletus*) occurs along the coast of Europe from the South of Norway [Wheeler, 1978] and the North of the Scotland [Gordon, 1981] to Gibraltar, also along the northern part of West Africa to Dakar, in the Mediterranean and Black Seas. Striped red mullet has been extensively studied in terms of quantity in the Mediterranean Sea and some studies were carried out in the Bay of Biscay [Desbrosses, 1933, 1935; N'Da and Deniel, 1993] that correspond to oldest exploitation areas in the Atlantic Ocean. Within the Atlantic Ocean, there are two main areas where this species is caught in this region: Bay of Biscay and in the Eastern English Channel. This species has been initially exploited by the Spanish fleets along their coast to the Bay of Biscay. Initially considered as a valuable by catch

[Marchal, 2008], the development of striped red mullet exploitation and a strong increase in landings along the English Channel and the southern North Sea by French, English and Dutch fleets have been observed since the 1990's. The strong increase of catches is essentially due to French trawlers and supplemented by the Netherlands and United Kingdom fleets which are carried out in the Eastern Channel and the south of North Sea [Mahé et al., 2005]. This could be attributed to an expansion of its migration distribution, abundance of this species coupled by the decline of traditionally targeted species in these areas and the sea-water warming trend [ICES, 2010; Marchal, 2008; Poulard and Blanchard, 2005]. Reports indicate a steady increase in East English Channel landings reaching ten times recorded landings in 1990 [Carpentier et al., 2009; Marchal, 2008]. Striped red mullet is still considered as a non-quota species in the Northeast Atlantic region and evaluation of the level of stock exploitation has only started since 7 years [ICES, 2010].

Stock identification and spatial structure information provide a basis for understanding fish population dynamics and provides reliable resource assessment for fishery management [Reiss et al., 2009]. Each stock may have unique demographic properties and responses or rebuilding strategies to exploitation. Biological attributes and productivity of species may be affected if the stock structure and fisheries management are not well considered [Smith et al., 1991].

There are a variety of techniques for stock identification such as genetics and morphometry studies. Genetic studies have been carried out in the Mediterranean Sea [Apostolidis et al., 2009; Galarza et al., 2009; Mamuris et al., 1998a,b]. In the Gulf of Pagasitikos (Greece sea), the analyses of three molucar markers revealed that this is a panmictic population [Apostolidis

et al., 2009]. However, on the level of the Mediterranean basin, the siculo-Tunisian Strait seems to be the transition zone between the Mediterranean's eastern and western populations [Galarza et al., 2009]. A sharp genetic division was detected when comparing striped red mullet originating from the Atlantic Ocean and from Mediterranean Sea.

Among all available techniques, otolith shape has been proven to be relevant feature for species and/or stock discrimination issues [Begg and Brown, 2000; Burke et al., 2008; Campana and Casselman, 1993; Stransky, 2005; Stransky et al., 2008b]. Otolith shape reflects the growth pattern of the fish as well as being markedly species specific. As a result, otolith shape can be used to differentiate stocks of the same species. Another relevant feature for stock identification is the growth law as growth is highly correlated to the environmental conditions and is thus stock specific.

In the present study, the stock identification was investigated with two methods based either on otolith shape or on growth marks (and both information). Images in reflected and transmitted light were acquired from 800 otoliths sampled in the Northwest European seas from South Bay of Biscay to North Sea. Growth marks have been pointed out manually by an expert. External shapes were extracted by computer vision process and then three automatic classification methods were compared, two classical state-of-the-art methods based on Fourier descriptors, Principal Component Analysis (PCA), and a recently proposed method [Nasreddine et al., 2009] based on shape geodesics.

2. Materials and methods

2.1. Otolith datasets

Striped red mullet otoliths were extracted from fish randomly sampled from the southern bay of Biscay to the North sea. The study area was divided into six geographic sectors: the NS (North Sea ; ICES Division IVab), the EEC (Eastern English Channel ; ICES Division VIId), the WEC (Western English Channel ; ICES Division VIIe), the CS (Celtic Sea ; ICES Division VIIh), the NBB (North Bay of Biscay ; ICES Division VIIIa) and the SBB (South Bay of Biscay ; ICES Division VIIIb) (Figure .1). All sampling were collected from September to December 2009 except the EEC otoliths which were collected from October-November 2007 and 2008.

{Figure .1 goes here }

The otoliths were selected from the routine surveys on board the RV "Thalassa" and RV "Gwen-Drez" conducted by the Ifremer Institute (France) and from fisheries markets. Fish were caught by otter trawl, bottom pair trawl and set gillnets. Both sagittal otoliths were removed and cleaned before drying and storing in paper envelope. One otolith per fish was examined using a light microscope connected to a video camera and a dedicated image-analysis system TNPC (digital processing for calcified structures) developed by Ifremer, ENIB and Noesis society.

Images of whole otoliths have been acquired using both transmitted and reflected lights. From 800 otoliths coming from six different stocks of striped red mullet (Figure .1), four different image datasets will be considered:

Dataset (1) : 600 otoliths sampled from six different stocks (100 otoliths per stock):

- NS: North Sea (IVab) - 2009

- EEC08: Eastern English Channel (VIId) - 2008
- WEC: Western English Channel (VIIe) - 2009
- CS: Celtic Sea (VIIh) - 2009
- NBB: North Bay of Biscay (VIIIa) - 2009
- SBB: South Bay of Biscay (VIIIb) - 2009

Dataset (2) : 700 otoliths: the 600 otoliths of dataset (1) with 100 other otoliths from Eastern English Channel but of a different year:

- EEC07: Eastern English Channel (VIId) - 2007

Dataset (3) : 200 otoliths: those from Eastern English Channel (VIId) over the two consecutive years 2007 and 2008:

- EEC07: Eastern English Channel (VIId) - 2007
- EEC08: Eastern English Channel (VIId) - 2008

Dataset (4) : 200 otoliths from North Sea (IVab) from the same year 2009 randomly divided in 2 classes:

- NS09a: North Sea (IVab) - 2009 a
- NS09b: North Sea (IVab) - 2009 b

These datasets illustrate two different types of applications of otolith shape classification: stock discrimination (datasets (1) and (2)) and year discrimination (datasets (3) and (4)). Both issues are quite hard for current state-of-the-art computer vision techniques because the external shapes of the considered otoliths exhibit very few differences.

For the year discrimination issue, the test is carried out on dataset (3) and dataset (4) separately. As dataset (4) is composed of randomized

classes, the classification performances on this dataset should be close to those of a theoretical random classifier (i.e. 50%). The difference in performances between dataset (3) and dataset (4) will give an idea of the validity of the results.

2.2. Shape-based stock identification

The shape-based classification process can be decomposed in three main steps (Figure .2). First, the otolith contour is extracted as described in next section (§ 2.2.1) using an automatic threshold. Three approaches to extract reduced-dimension feature vectors from the contours were considered: Fourier Transform (FT), Principal Component Analysis (PCA) and a technique issued from shape geodesics [Nasreddine et al., 2009]. The discriminative power of each approach is evaluated using its own distance matrix as input for a classifier. In other words, for a query input the feature vector is considered as the distance matrix calculated between this individual and the training individuals. Here, we investigate the performances of two widely used classifiers: (1) the K-Nearest Neighbors (KNN) classifier with the "leave-one-out" heuristic and (2) the Support Vector Machine (SVM) classifier [Vapnik, 1995] with two randomly-selected sub-samples, one of them is used to build the SVM-model which is tested on the other.

{Figure .2 goes here }

2.2.1. Automatic contour extraction

The otolith image is acquired using two imaging modalities: by transmitted light or by reflected light. These two modalities could give additional information. To extract the otolith outline, a mixed image is built in order to integrate information available in both modalities (Figure .3). This mixed

image is a mean between the transmitted light image and the negative of the reflected light image. Image contours are detected as local maximum of the image gradient, approximated using a Sobel filtering. The resulting contours are filled by a morphological closing operation and filtered to retain the largest connected component which corresponds to the edge of the otolith. The advantage of mixing both image modalities is illustrated on example given by figure .3. The mixed image gives more details about the contour especially on the region of the excisura major.

{Figure .3 goes here }

The resulting contour is then sampled into 300 points which describe adequately the otolith shape.

2.2.2. Fourier descriptors

Shape can be described using complex Fourier descriptors [Granlund, 1972] or using elliptic Fourier descriptors [Kuhl and Giardina, 1982]. For otolith shape analyses, both techniques have been extensively used and proved to be efficient [Duarte-Neto et al., 2008a; Kristoffersen and Magoulas, 2008; Mérigot et al., 2007; Stransky et al., 2008a] [Cardinale et al., 2004; Galley et al., 2006; Robertson and Talman, 2002; Schulz-Mirbach et al., 2008; Smith, 1992; Torres et al., 2000]. In our previous work [Nasreddine et al., 2009] we have showed that for red mullet otoliths, classification results are still similar by using these two methods. Elliptic Fourier descriptors are more appropriate than complex Fourier descriptors when otolith contours are composed of series of ellipse arcs (as for Trachurus mediterraneus otoliths for example). Hence, for striped red mullet otoliths we have chosen to use the complex descriptors which can be implemented more efficiently.

With a view to achieving translation, rotation and scaling invariance,

the first descriptor is aborted and the selected descriptors are scaled with respect to the first non zero coefficient resulting in the so-called *normalized Fourier descriptors*. The distance between two shapes is computed as the Euclidean distance between the associated vectors of the normalized Fourier descriptors.

2.2.3. Principal Component Analysis (PCA)

Principal Component Analysis (PCA) was first introduced by Pearson in [Pearson, 1901] as a mathematical tool that transforms data linearly correlated to uncorrelated variables called principal components. PCA is extensively used in fisheries research for otolith shape analyses, in particular for otolith stock identification. Usually, PCA is applied on Fourier coefficients in order to assess differences in otolith shape [Duarte-Neto et al., 2008b; Mérigot et al., 2007; Schulz-Mirbach et al., 2008]. PCA can also be applied on morphometric variables [Torres et al., 2000], on a binary low resolution image of the contour [Bermejo and Monegal, 2007] or for standardizing the otolith contour orientation [Piera et al., 2005].

However, PCA is not invariant to affine transformations, it is applied for pattern recognition when the coordinates of input vectors can be ordered. In face recognition for example, eyes and lips centers are manually selected, then the images are rotated, in order to make the line connecting eye centers horizontal, and resized to make the distances between the centers of the eyes equal. The PCA is carried out on data vectors formed by cropped part of images. In the case of calcified structures, it is not always obvious to order the data vector coordinates on the basis of clearly defined landmarks. A normalization procedure should then be applied to the raw contours to be invariant with respect to translation, rotation and scaling, so that the

normalized shape is the result of the fish history, independently of acquisition settings.

The translation invariance is obtained simply by subtracting the coordinates of the mass center to the coordinates of all points. Scale invariance is also simply obtained by dividing each point of the contour in polar coordinates by the mean radius. For rotation normalization, a first solution could be to align shapes according to the main axis. This axis can be defined by the two farthest points of the shape or by minimizing the covariance using a PCA like in [Piera et al., 2005]. However, on striped red mullet otolith, the main axis does not correspond to a meaningful biological feature. Instead, we propose to normalize shapes according to the center of excisura major.

The corresponding point of the excisura major can be detected automatically after subtraction of the original otolith shape from the corresponding filled shape. Then, each shape is aligned according to the axis that passes through this point and the mass center of the otolith contour (Figure .4).

{Figure .4 goes here }

After contours normalization, PCA is applied on a matrix where each of the rows represents a different contour and the columns represent the information about the contours: the Cartesian normalized coordinates and the local curvature are all put together in a row, one after the other.

To compute a distance between all contours in a given dataset, we proceed with a "leave-one-out" heuristics. One after another, each contour C_i of the dataset is left out and PCA is computed on the remaining contours. Then contour C_i is projected into the eigenspace generated by the eigenvectors. Finally the distances between the projected contour and each of the other projected contours of the dataset are computed as Euclidean distances in the eigenspace.

2.2.4. The geodesics approach

A potential drawback of Fourier and PCA approaches comes from the implicit global (spatial) characterization of the shape. Each descriptor holds information about all points of the shape as it is calculated using all points. Therefore, local (spatial) discriminant shape signatures, such as shape discontinuities or landmarks, may not be well exploited by such a global characterization [Parisi-Baradad et al., 2005]. In contrast, a Geodesic approach was recently proposed [Nasreddine et al., 2009] to take advantage of local shape features while ensuring invariance to geometric transformations (e.g. translation, rotation and scaling). In this approach, we have defined distance between shapes as a deformation cost stated as a matching issue, i.e. determining the optimal matching between two otolith contours with respect to a similarity measure.

The distance $d(\Gamma_1, \Gamma_2)$ between two shapes Γ_1 and Γ_2 is stated as the minimum, over all mapping functions Ψ, of the similarity measure, $E_D(\Gamma_1, \phi(\Gamma_2))$ between the reference shape Γ_1 and the mapped shape $\phi(\Gamma_2)$.

$$d(\Gamma_1, \Gamma_2) = \min_{\phi \in \Psi} E_D(\Gamma_1, \phi(\Gamma_2)) \quad (1)$$

As the important biological information is considered in the shape of contour and not in its size, the shapes are parameterized in function of the normalized curvilinear abscissa s which has a value between 0 and 1 independently of the original contour length. A robust criterion is introduced in order to improve the robustness of the proposed distance to outliers coming from biological interindividual variabilities. The principle is supported by the use of a function that adjusts weight ω in order to penalize the data points of high variation compared to other points.

Given two shapes locally characterized by the angle $\theta(s)$ between the tangent to the curve and the horizontal axis, the distance between two contours is defined by:

$$d(\theta_1(s), \theta_2(s)) = 2 \inf_{\phi} \arccos \int_s \sqrt{\phi_s(s)} \left| \cos \frac{\omega(r(s))r(s)}{2} \right| ds \qquad (2)$$

where $\phi_s = \frac{d\phi}{ds}$ and $r(s) = \theta_1(s) - \theta_2(\phi(s))$. The term $\sqrt{\phi_s(s)}$ allows to avoid torsion and stretching along the curve. The weight function ω is issued from the robust estimator of Leclerc [Black and Rangarajan, 1996]; $\omega(r(s)) = \frac{2}{\sigma^2} exp(\frac{-r^2(s)}{\sigma^2})$ where σ is the standard deviation of data errors $r(s)$.

Formally, the numerical computation of $d(\Gamma_1, \Gamma_2)$ is solved by using a dynamic programming technique (refer to [Nasreddine et al., 2009] for more details).

2.3. Growth marks based stock identification

The growth-based classification process consists of three main steps (Figure .2). First, an expert manually points out the growth marks on the otolith image (Figure .5). This step can be done using **TNPC** software (www.tnpc.fr) in parallel with the image acquisition step; it is not a contradiction with the automatic process of classification. Then distance between the growth laws of two otoliths is computed using the Euclidean distances between growth vectors. In case of two different aged otoliths, distance is computed using only the growth marks available on both otoliths. For example, in figure .5 this distance is computed using the three growth marks on each otolith.

Given two growth vectors $G_1 = \{G_{1j}\}_{j=1\cdots N_1}$ and $G_2 = \{G_{2j}\}_{j=1\cdots N_2}$, the growth distance is considered as the Euclidean distance:

$$d_{Growth} = \sqrt{\sum_{j=1}^{N_g} (G_{2j} - G_{1j})^2} \quad (3)$$

where $N_g = \mathbf{min}\{N_1, N_2\}$ is the number of growth marks available in both vectors.

Finally, all distances between otoliths are computed leading to a distance matrix used as input for an SVM classifier. The feature vector is considered as the distance calculated between the query input and all training individuals.

{Figure .5 goes here }

3. Results

Here performances are evaluated in terms of correct classification rates. We have started experiments with the hypothesis that the six stocks (NS, EEC, WEC, CS, NBB and SBB) are considered as individual separated stocks with specific characteristics of shapes.

Compared to KNN, SVM classifier performs slightly better in terms of correct classification rate (from 30% to 32.7% on dataset (1)) but at the cost of increasing dramatically the standard deviation of the performances between classes (from 10.9 to 15.2 on dataset (1)). Thus, as KNN classifier results in stable performances across the classes, it has been chosen for shape-based classification. In contrast, applying KNN for growth-based stock identification gives a correct classification rate of 25.5% whereas SVM gives higher correct classification rate (35.4%) for the same dataset (dataset (1)). Hence, SVM has been chosen for growth-based classification.

The correct classification rates remain high with respect to the random classification but these rates show that the hypothesis of separated stocks

should be aborted. The six stocks are then grouped into three stocks leading to a correct classification rate of 67%. Grouped stocks have in the first hypothesis close shape characteristics and could not be really distinguished easily. Classification errors could be due to genetic factors, migration among others. A rate of 100% could then not be reached with the presence of all these factors on the otolith shape. In comparisons to other stock identification methods, otolith shape is a promising approach but interpreting patterns of variance can be difficult [Cadrin et al., 2005].

In the following, geographical zones are ordered in the tables according to their positions (from north (NS) to south (SBB)); thus neighbor classes are also neighbor geographical zones.

3.1. Dataset (1)

Results on dataset (1) are given in tables .1-.3. Geodesic approach reaches 30% of correct classification (Table .3) while this rate is 19.7% for Fourier approach (Table .1) and 25% for PCA (Table .2). These scores are better than a random classification that would theoretically reach 16.7% (for six classes).

{Table .1 goes here }

{Table .2 goes here }

{Table .3 goes here }

In table .4, classification results are given when the growth information is used for stock identification. The mean correct classification obtained by SVM reaches 35.4%.

{Table .4 goes here }

As in [Nasreddine et al., 2009], we have tested stock identification with both growth and shape information in order to improve classification per-

formances. The mean correct classification rate is then increased to reach 49.4% (Table .5).

{Table .5 goes here }

3.2. Dataset (2)

On dataset (2), Fourier approach reaches 16.4% of mean correct classification (Table .6), PCA approach reaches 19% of correct classification (Table .7) while Geodesic approach reaches 24.9% (Table .8). These scores are also better than a random classification that would theoretically reach 14.3% (for seven classes).

{Table .6 goes here }

{Table .7 goes here }

{Table .8 goes here }

3.3. Datasets (3) and (4)

Regarding the year discrimination issue on dataset (3), the mean classification rate of the Fourier approach (56%, Table .9) is too close to the theoretical mean classification rate of a random classifier (50% for two classes). Thus the classical Fourier approach fails on this specific year discrimination issue. The mean classification rate on the random dataset (4) (43%, Table .10) is lower but quite close to the theoretical mean classification rate of a random classifier (50% for two classes), it shows that with this approach, two arbitrary sets of the same stock and same year have no significant shape differences.

Regarding PCA and Geodesic approaches, the mean classification rate on dataset (3) (60%, Table .9) is higher than the mean classification rate on the random dataset (4) (49.5%, Table .10). This shows that the otolith

morphology varies over two consecutive years and that this difference in shape is higher than between two arbitrary groups of the same year and same stock.

{Table .9 goes here }

{Table .10 goes here }

4. Discussion

4.1. Comparison of the three shape-based approaches

Performances of the three shape-based approaches are compared in table .11. On both dataset (1) and dataset (2), the Geodesic approach exhibits highest performances followed by PCA approach and Fourier approach last.

Regarding the stock discrimination issue on dataset (1) (Tables .1, .2 and .3), the three methods show that the population of striped red mullet can be geographically divided in three zones:

- The Bay of Biscay (NBB+SBB)
- A mixing zone composed of the Celtic Sea and the Western English Channel (CS+WEC)
- A northern zone composed of the Eastern English Channel and the North Sea (EEC+NS)

To further the "three zones" hypothesis, we have tested the classification when the otoliths were grouped in three classes corresponding to the three zones. The results of this classification using the geodesic approach is shown in table .12 below. It clearly validates the hypothesis as the obtained mean correct classification rate reaches 54.3% and the error scores are higher between two neighbors zones than between two unconnected zones. Finally,

this rate raises to 67.31% when the SVM classifier is used with geodesic distances coupled with the growth information (Table .13).

Regarding the year discrimination issue, classical Fourier approach fails while PCA approach shows a small difference in shape and Geodesic approach exhibits the highest difference (Table .11). Thus Geodesic approach seems the most appropriate method for this task.

{Table .11 goes here }

{Table .12 goes here }

{Table .13 goes here }

4.2. Relevance of the shape and growth information

In this study three different approaches have been compared for shape-based stock identification, two state-of-the-art methods (Fourier and PCA) that have been extensively used in marine research on different species, and a recent method (Geodesic) that proved to give very good performances on different shapes [Nasreddine et al., 2010] and in particular on otolith shapes [Nasreddine et al., 2009]. Although these three methods result in high correct classification rates on several problems, they give quite low correct classification rate for the particular cases tested in this study. It tends to prove that otolith shape is not relevant for the particular case of striped red mullet if we consider the six stocks separately. The growth-based stock identification results are not so far from the shape-based stock identification results. This study shows that both information are influenced by different living conditions and different environments and can serve as stock identifier. This identification is not very high as otolith shape is highly due to the genetics. This result tends to prove that the genetic information is quite homogeneously spread across all geographical zones in the north

west European seas.

This study has proven that by coupling both information (shape and growth patterns), stock discrimination becomes more efficient. These two information are independent and multivariate analysis, including them with other independent information (chemical concentrations, ...), should be investigated for stock identification.

The observations above lead to two hypothesis on the striped red mullet:

- some adults move from one zone to another,
- some larvae or juveniles perform migration during growth.

Acknowledgement

The authors want to thank the European commission for providing the financial support of this work through the NESPMAN project, all scientists and crew on board the RV "Thalassa" and the RV "Gwen Drez" for their help with sample collection.

Apostolidis, A., Moutou, K., Stamatis, C., Mamuris, Z., 2009. Genetic structure of three marine fishes from the gulf of pagasitikos (greece) based on allozymes, RAPD, and mtDNA RFLP markers. Biologia 64 (5), 1005–1010.

Begg, G., Brown, R., 2000. Stock identification of haddock melanogrammus aeglefinus on georges bank based on otolith shape analysis. Transactions of the American Fisheries Society 129, 935–945.

Bermejo, S., Monegal, B., 2007. Fish age analysis and classification with kernel methods. Pattern Recognition Letters 28 (10), 1164–1171.

Black, M., Rangarajan, A., 1 1996. On the unification of line processes, outlier rejection, and robust statistics with applications in early vision. International Journal of Computer Vision 19 (5), 57–92.

Burke, N., Brophy, D., King, P., 2008. Otolith shape analysis: its application for discriminating between stocks of irish sea and celtic sea herring (clupea harengus) in the irish sea. ICES Journal of Marine Science 65.

Cadrin, S., Friedland, K., Waldman, J., 2005. Stock identification methods: Applications in Fishery science. Elsevier Academic press.

Campana, S., Casselman, J., 1993. Stock discrimination using otolith shape analysis. Canadian Journal of Fisheries and Aquatic Sciences 50, 1062–1083.

Cardinale, M., Doering-Arjes, P., Kastowsky, M., Mosegaard, H., 2004. Effects of sex, stock, and environment on the shape of known-age atlantic cod (gadus morhua) otoliths. Canadian Journal of Fisheries and Aquatic Sciences 61 (2), 158–167.

Carpentier, A., Martin, C., Vaz, S., 2009. Channel habitat atlas for marine resource management (charm phase ii). INTERREG 3a Programme, IFREMER, Boulogne-sur-mer 65.

Desbrosses, P., 1933. Contribution à la biologie du rouget-barbet en atlantique nord. Revue des Travaux de l'Institut des Pêches Maritimes 6 (3), 249–270.

Desbrosses, P., 1935. Contribution à la connaissance de la biologie du rouget barbet en atlantique nord (iii) mullus barbatus (rond) surmuletus fage

mode septentrional fage. Revue des Travaux de l'Institut des Pêches Maritimes 8 (4), 351–376.

Duarte-Neto, P., Lessa, R., Stosic, B., Morize, E., 2008a. The use of sagittal otoliths in discriminating stocks of common dolphinfish (coryphaena hippurus) off northeastern brazil using multishape descriptors. ICES Journal of Marine Science 65 (7), 1144–1152.

Duarte-Neto, P., Lessa, R., Stosic, B., Morize, E., 2008b. The use of sagittal otoliths in discriminating stocks of common dolphinfish (coryphaena hippurus) off northeastern brazil using multishape descriptors. ICES Journal of Marine Science 65, 1144–1152.

Galarza, J., Turner, G., Macpherson, E., Rico, C., 2009. Patterns of genetic differentiation between two co-occurring demersal species: the red mullet (mullus barbatus) and the striped red mullet (mullus surmuletus). Canadian Journal of Fisheries and Aquatic Sciences 66 (9), 1478–1490.

Galley, E. A., Wright, P. J., Gibb, F. M., 2006. Combined methods of otolith shape analysis improve identification of spawning areas of Atlantic cod. ICES Journal of Marine Science 63 (9), 1710–1717.

Gordon, J., 1981. The fish populations of the west of scotland shelf. Part II, Oceanography and Marine Biology. Annual Review 19, 405–441.

Granlund, G., 1972. Fourier preprocessing for hand print character recognition. IEEE Transanctions on Computers C-21, 195–201.

ICES, 2010. Report of the working group on assessment of new MoU species (WGNEW). Tech. rep., ICES CM 2010/ACOM: 21.

Kristoffersen, J., Magoulas, A., 2008. Population structure of anchovy engraulis encrasicolus L. in the mediterranean sea inferred from multiple methods. Fisheries research 91 (2-3), 187–195.

Kuhl, F., Giardina, C., 1982. Elliptic fourier features of a closed contour. Computer Graphics and Image Processing 18, 236–258.

Mahé, K., Destombes, A., Coppin, F., Koubbi, P., Vaz, S., Roy, D. L., Carpentier, A., 2005. Le rouget barbet de roche mullus surmuletus (L. 1758) en manche orientale et mer du nord. Rapp. Contrat Ifremer/CRPMEM Nord-Pas de Calais, 187p.

Mamuris, Z., Apostolidis, A., Theodorou, A., Triantaphyllidis, C., 1998a. Application of random amplified polymorphic dna (rapd) markers to evaluate intraspecific genetic variation in red mullet (mullus barbatus). Marine Biology 132, 171–178.

Mamuris, Z., Apostolidis, A., Triantaphyllidis, C., 1998b. Genetic protein variation in red mullet (mullus barbatus) and striped red mullet (m. surmuletus) populations from the mediterranean sea. Marine Biology 130, 353–360.

Marchal, P., 2008. A comparative analysis of metiers and catch profiles for some french demersal and pelagic fleets. ICES Journal of Marine Science 65, 674–686.

Mérigot, B., Letourneur, Y., Lecomte-Finiger, R., 2007. Characterization of local populations of the common sole Solea solea (Pisces, Soleidae) in the NW mediterranean through otolith morphometrics and shape analysis. Marine Biology 151 (3), 997–1008.

Nasreddine, K., Benzinou, A., Fablet, R., 2009. Shape geodesics for the classification of calcified structures: beyond fourier shape descriptors. Fisheries Research 98 (1-3), 8–15.

Nasreddine, K., Benzinou, A., Fablet, R., 2010. Variational shape matching for shape classification and retrieval. Pattern Recognition Letters 31 (12), 1650–1657.

N'Da, K., Deniel, C., 1993. Sexual cycle and seasonal changes in the ovary of the red mullet, mullus surmuletus, from the southern coast of brittany. Journal of Fish Biology 43 (2), 229–244.

Parisi-Baradad, V., Lombarte, A., Garcia-Ladona, E., Cabestany, J., Piera, J., Chic, O., 2005. Otolith shape contour analysis using affine transformation invariant wavelet transforms and curvature scale space representation. Marine and Freshwater Research 56, 795–804.

Pearson, K., 1901. On lines and planes of closest fit to systems of points in space. Philosophical Magazine 2 (6), 559–572.

Piera, J., Parisi-Baradad, V., Garcia-Ladona, E., Lombarte, A., Recasens, L., Cabestany, J., 2005. Otolith shape feature extraction oriented to automatic classification with open distributed data. Marine and freshwater research 56 (5), 805–814.

Poulard, J., Blanchard, F., 2005. The impact of climate change on the fish community structure of the eastern continental shelf of the bay of biscay. ICES Journal of Marine Science 62, 1436–1443.

Reiss, H., Hoarau, G., Dickey-Collas, M., Wolff, W., 2009. Genetic popula-

tion structure of marine fish: mismatch between biological and fisheries management units. Fish and Fisheries 10, 361–395.

Robertson, S., Talman, S., 2002. Shape analysis and ageing of orange roughy otoliths from the south tasman rise. Tech. rep., Final Report to the Australian Fisheries Management Authority. Marine and Freshwater Resources Institute.

Schulz-Mirbach, T., Stransky, C., Schlickeisen, J., Reichenbacher, B., 2008. Differences in otolith morphologies between surface- and cave-dwelling populations of Poecilia mexicana (teleostei, poeciliidae) reflect adaptations to life in an extreme habitat. Evolutionary Ecology Research 10 (4), 537–558.

Smith, M. K., 1992. Regional differences in otolith morphology of the deep slope red snapper etelis carbunculus. Canadian Journal of Fisheries and Aquatic Sciences 49 (4), 795–804.

Smith, P., Francis, R., McVeagh, M., 1991. Loss of genetic diversity due to fishing pressure. Fisheries Research 10, 309–316.

Stransky, C., 2005. Geographic variation of golden redfish (sebastes marinus) and deep-sea redfish (s. mentella) in the north atlantic based on otolith shape analysis. ICES Journal of Marine Science 62, 1691–1698.

Stransky, C., Baumann, H., Fevolden, S.-E., Harbitz, A., Hie, H., Nedreaas, K. H., Salberg, A.-B., Skarstein, T. H., 2008a. Separation of norwegian coastal cod and northeast arctic cod by outer otolith shape analysis. Fisheries Research 90 (1-3), 26–35.

Stransky, C., Murta, A., Schlickeisen, J., Zimmermann, C., 2008b. Otolith shape analysis as a tool for stock separation of horse mackerel (trachurus trachurus) in the northeast atlantic and mediterranean. Fisheries Research 89, 159–166.

Torres, G. J., Lombarte, A., Morales-Nin, B., 2000. Sagittal otolith size and shape variability to identify geographical intraspecific differences in three species of the genus merluccius. Journal of the Marine Biological Association of the UK 80 (2), 333–342.

Vapnik, V., 1995. The nature of statistical learning theory. Springer-Verlag, New York, USA.

Wheeler, A., 1978. Key to the fishes of northern europe. Frederick Warne & Co. Ltd Londres, 380p.

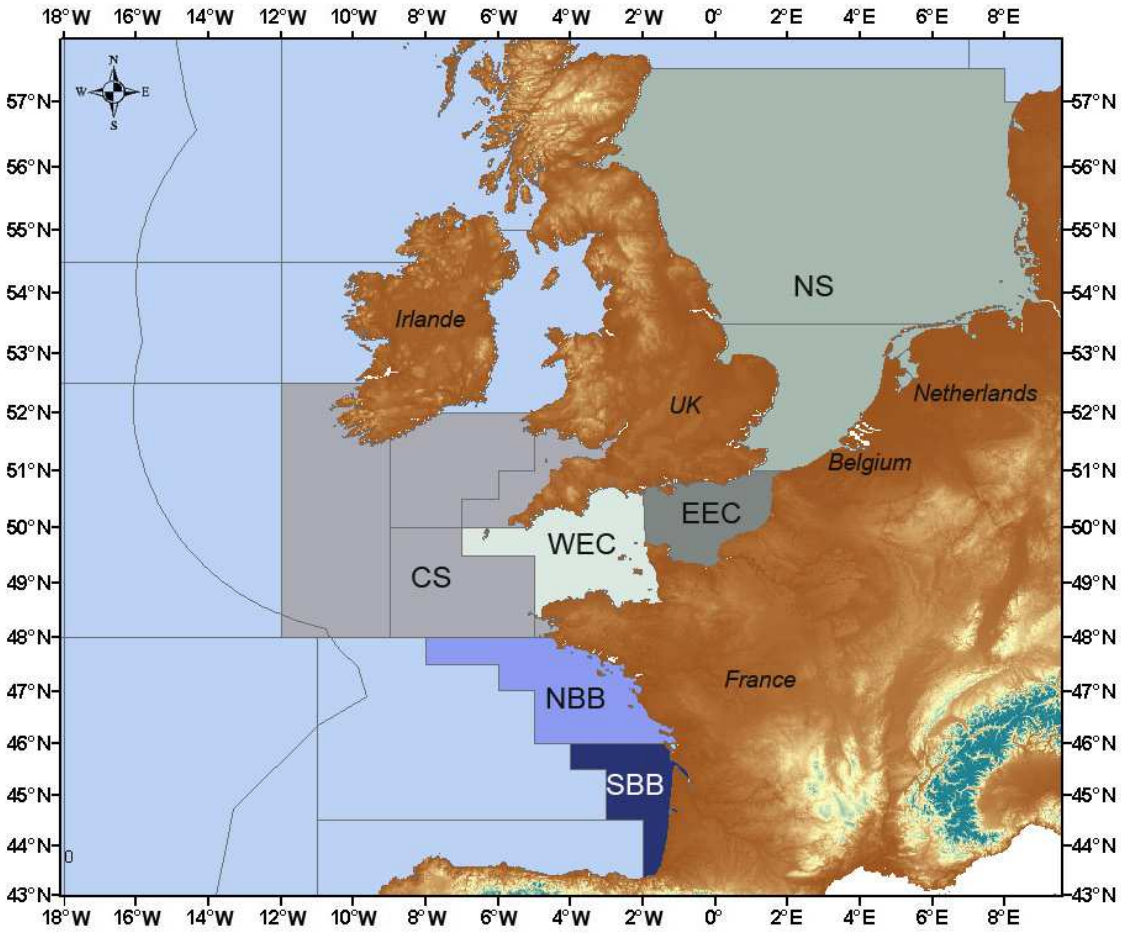

Figure .1: Map of the stocks of striped red mullet involved in this study.

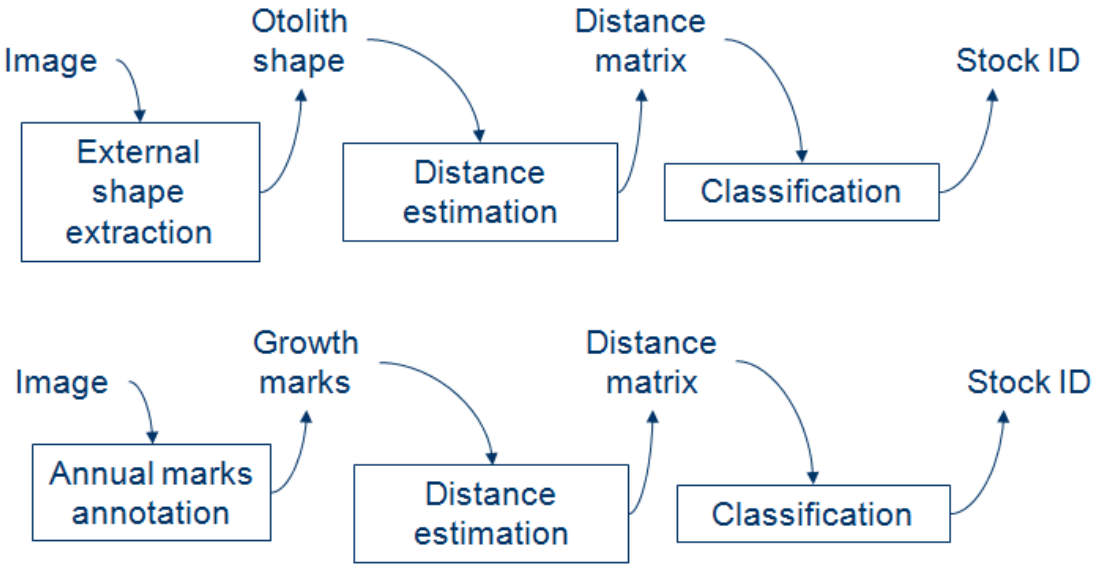

Figure .2: Shape-based and growth-based classification general schemes.

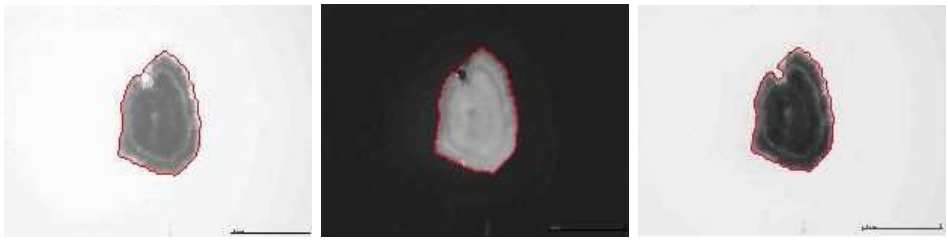

Figure .3: Contour extraction using transmitted light image (left), reflected light image (middle) and resulting mixed image (right). Note that the contour extracted using the mixed image is more efficient.

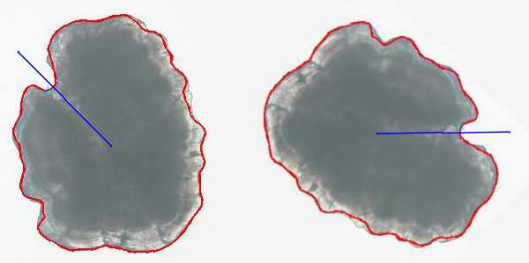

Figure .4: Contour extraction and normalization. Left: contour before normalization, right: contour after rotation normalization. In this figure we show the main axis passing through the mass center and the excisura major center.

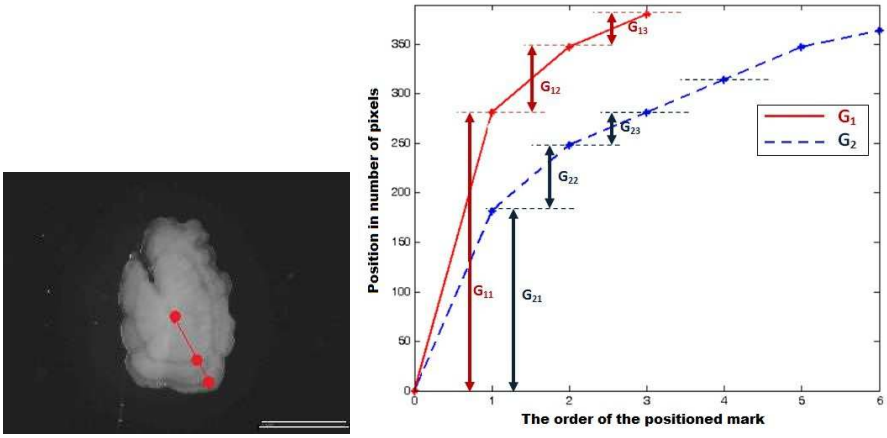

(a) (b)

Figure .5: Illustration of growth distance calculation. (a): Annual growth marks manually positioned by expert. (b): Example of distance computation between growth laws of two otoliths.

Table .1: Confusion matrix (in %) for the Fourier approach on dataset (1) achieved by KNN classifier. Mean correct classification rate: 19.7%.

Fourier approach on Dataset (1)						
	Actual Class					
Estimated Class	**NS**	**EEC08**	**WEC**	**CS**	**NBB**	**SBB**
NS	**18**	20	11	18	18	12
EEC08	21	**28**	25	17	6	14
WEC	8	19	**12**	16	7	14
CS	21	12	18	**13**	11	14
NBB	16	9	14	16	**23**	22
SBB	16	12	20	20	35	**24**

Table .2: Confusion matrix (in %) for the PCA approach on dataset (1) achieved by KNN classifier. Mean correct classification rate: 25%.

PCA approach on Dataset (1)						
	Actual Class					
Estimated Class	**NS**	**EEC08**	**WEC**	**CS**	**NBB**	**SBB**
NS	**29**	13	15	19	10	12
EEC08	18	**31**	16	21	10	10
WEC	14	13	**26**	11	21	18
CS	17	21	15	**20**	11	12
NBB	15	11	12	13	**21**	25
SBB	7	11	16	16	27	**23**

Table .3: Confusion matrix (in %) for the Geodesic approach on dataset (1) achieved by KNN classifier. Mean correct classification rate: 30%.

Geodesic approach on Dataset (1)						
	Actual Class					
Estimated Class	**NS**	**EEC08**	**WEC**	**CS**	**NBB**	**SBB**
NS	**15**	20	11	8	5	11
EEC08	28	**44**	17	23	5	5
WEC	9	9	**22**	11	7	9
CS	24	15	24	**32**	15	13
NBB	10	5	16	13	**27**	22
SBB	14	7	10	13	41	**40**

Table .4: Confusion matrix resulting from an SVM classifier on growth distances (dataset (1)). Mean correct classification rate: 35.4 %.

Growth-based approach on Dataset (1)						
Estimated	**Actual class**					
class	**NS**	**EEC08**	**WEC**	**CS**	**NBB**	**SBB**
NS	**42.49**	20.34	16.58	5.62	3.84	11.13
EEC08	12.30	**50.38**	13.12	2.36	5.56	16.28
WEC	12.14	19.26	**41.35**	5.13	8.54	13.58
CS	41.7	2.74	43.71	**8.74**	3.33	0.29
NBB	11.47	8.79	30.07	3.66	**26.47**	19.54
SBB	12.02	20.12	12.00	1.39	11.12	**43.34**

Table .5: Confusion matrix resulting from an SVM classifier on geodesic distances coupled with growth distances (dataset (1)). Mean correct classification rate: 49.4 %.

Growth and Geodesic-based approach on Dataset (1)						
Estimated	**Actual class**					
class	**NS**	**EEC08**	**WEC**	**CS**	**NBB**	**SBB**
NS	**43.75**	12.00	2.44	12.25	5.00	3.57
EEC08	31.25	**66.00**	21.95	18.36	0.00	0.00
WEC	12.50	16.00	**60.98**	4.08	0.00	25
CS	8.33	6.00	9.76	**44.89**	20.00	10.71
NBB	0.00	0.00	2.44	20.41	**45.00**	25.00
SBB	4.17	0.00	2.44	0.00	30.00	**35.71**

Table .6: Confusion matrix (in %) for the Fourier approach on dataset (2) achieved by KNN classifier. Mean correct classification rate: 16.4%.

Fourier approach on Dataset (2)							
	Actual Class						
Estimated Class	**NS**	**EEC07**	**EEC08**	**WEC**	**CS**	**NBB**	**SBB**
NS	**15**	10	22	7	18	13	11
EEC07	15	**19**	12	23	14	11	11
EEC08	17	16	**24**	18	17	7	11
WEC	6	17	14	**7**	14	5	11
CS	20	14	8	17	**7**	12	11
NBB	16	14	8	12	15	**20**	22
SBB	11	10	12	16	15	32	**23**

Table .7: Confusion matrix (in %) for the PCA approach on dataset (2) achieved by KNN classifier. Mean correct classification rate: 19%.

PCA approach on Dataset (2)							
	Actual Class						
Estimated Class	**NS**	**EEC07**	**EEC08**	**WEC**	**CS**	**NBB**	**SBB**
NS	**20**	10	11	17	14	8	7
EEC07	16	**15**	17	8	14	16	14
EEC08	12	15	**24**	14	16	8	7
WEC	12	16	14	**22**	14	16	13
CS	19	12	16	14	**15**	11	9
NBB	13	19	9	10	14	**15**	28
SBB	8	13	9	15	13	26	**22**

Table .8: Confusion matrix (in %) for the Geodesic approach on dataset (2) achieved by KNN classifier. Mean correct classification rate: 24.9%.

Geodesic approach on Dataset (2)							
	Actual Class						
Estimated Class	**NS**	**EEC07**	**EEC08**	**WEC**	**CS**	**NBB**	**SBB**
NS	**10**	13	16	8	7	2	10
EEC07	23	**32**	22	27	28	19	13
EEC08	23	15	**36**	13	17	6	5
WEC	5	3	5	**15**	9	4	7
CS	18	13	13	16	**24**	10	11
NBB	9	13	3	12	6	**23**	20
SBB	12	11	5	9	9	36	**34**

Table .9: Confusion matrix (in %) on dataset (3) achieved by KNN classifier. Mean correct classification rate: 56% with the Fourier approach, 60% by the PCA approach and 60.5% with the Geodesic approach.

Year discrimination on Dataset (3)		
by Fourier approach		
	Actual Class	
Estimated Class	**EEC07**	**EEC08**
EEC07	**54**	42
EEC08	46	**58**
by PCA approach		
	Actual Class	
Estimated Class	**EEC07**	**EEC08**
EEC07	**58**	38
EEC08	42	**62**
by Geodesic approach		
	Actual Class	
Estimated Class	**EEC07**	**EEC08**
EEC07	**64**	43
EEC08	36	**57**

Table .10: Confusion matrix (in %) on dataset (4) achieved by KNN classifier. Mean correct classification rate: 43% with the Fourier approach, 49.5% by the PCA approach and 49.5% with the Geodesic approach.

Validation test on Dataset (4)		
by Fourier approach		
	Actual Class	
Estimated Class	**NS09a**	**NS09b**
NS09a	**43**	57
NS09b	57	**43**
by PCA approach		
	Actual Class	
Estimated Class	**NS09a**	**NS09b**
NS09a	**46**	47
NS09b	54	**53**
by Geodesic approach		
	Actual Class	
Estimated Class	**NS09a**	**NS09b**
NS09a	**54**	55
NS09b	46	**45**

Table .11: Comparison of the mean correct classification rate (in %) obtained by the three approaches on datasets (1), (2) and (3) achieved by KNN classifier.

	dataset (1)	**Dataset (2)**	**Dataset (3)**
Fourier	19.7	16.4	56
PCA	25	19	60
Geodesic	30	24.9	60.5

Table .12: Classification results on dataset (1) with the Geodesic approach when the otoliths were grouped in three classes according to their geographical zones. Mean correct classification rate: 54.3% (KNN classifier).

Geodesic approach on Dataset (1) with otoliths grouped by zones			
	Actual Class		
Estimated Class	**Northern zone**	**Mixing zone**	**Bay of Biscay**
Northern zone	**53.5**	29.5	13
Mixing zone	28.5	**44.5**	22
Bay of Biscay	18	26	**65**

Table .13: Classification results (in %) on dataset (1) with the Growth and Geodesic-based approach when the otoliths were grouped in three classes according to their geographical zones. Mean correct classification rate: 67.31% (SVM classifier).

Growth and Geodesic-based approach on Dataset (1) with otoliths grouped by zones			
	Actual Class		
Estimated Class	**Northern zone**	**Mixing zone**	**Bay of Biscay**
Northern zone	**74.30**	26.76	8.61
Mixing zone	22.31	**58.25**	22.00
Bay of Biscay	3.39	14.99	**69.39**